Eur Biophys J (2011) 40:727–736
DOI 10.1007/s00249-011-0685-4

ORIGINAL PAPER

# Hydrophobicity drives the cellular uptake of short cationic peptide ligands

**Anju Gupta · Deendayal Mandal · Yousef Ahmadibeni · Keykavous Parang · Geoffrey Bothun**

Received: 9 December 2010 / Revised: 2 February 2011 / Accepted: 16 February 2011 / Published online: 16 March 2011


**Abstract** Short cationic linear peptide analogs (LPAs, prepared as Arg-$C_n$-Arg-$C_n$-Lys, where $C_n$ represents an alkyl linkage with $n = 4$, 7 or 11) were synthesized and tested in human breast carcinoma BT-20 and CCRF-CEM leukemia cells for their application as targeting ligands. With constant LPA charge (+4), increasing the alkyl linkage increases the hydrophobic/hydrophilic balance and provides a systematic means of examining combined electrostatic and hydrophobic peptide–membrane interactions. Fluorescently conjugated LPA-$C_{11}$ (F-LPA-$C_{11}$) demonstrated significant uptake, whereas there was negligible uptake of the shorter LPAs. By varying temperature (4°C and 37°C) and cell type, the results suggest that LPA-$C_{11}$ internalization is nonendocytic and nonspecific. The effect of LPA binding on the phase behavior, structure, and permeability of model membranes composed of dipalmitoylphosphatidylcholine and dipalmitoylphosphatidylserine (DPPC/DPPS, 85/15) was studied using differential scanning calorimetry (DSC), cryogenic transmission electron microscopy (cryo-TEM), and fluorescence leakage studies to gain insight into the LPA uptake mechanism. While all LPAs led to phase separation, LPA-$C_{11}$, possessing the longest alkyl linkage, was able to penetrate into the bilayer and caused holes to form, which led to membrane disintegration. This was confirmed by rapid and complete dye release by LPA-$C_{11}$. We propose that LPA-$C_{11}$ achieves uptake by anchoring to the membrane via hydrophobicity and forming transient membrane voids. LPAs may be advantageous as drug transporter ligands because they are small, water soluble, and easy to prepare.

**Keywords** Cell-penetrating peptide · Lipid membrane · Phase separation · Calorimetry · Pore formation

## Introduction

Cell-penetrating peptides (CPP) are typically composed of 30 or fewer amino acids and possess the ability to traverse cellular membranes (Deshayes et al. 2005; El-Andaloussi et al. 2005; Patel et al. 2007; Stewart et al. 2008; Vives et al. 2008; Ziegler 2008). Since the plasma membrane protects cells from uncontrolled uptake of bioactive molecules, ligands or "molecular transporters" such as CPPs can be conjugated to therapeutic molecules and used to facilitate membrane translocation for intracellular delivery. Tat peptide, derived from the HIV-1 Tat transactivator protein, and penetratin, derived from the *Drosophila* antennapedia homeodomain, represent two well-known and naturally occurring CPPs that have been shown to be efficient transporters for membrane translocation (Fawell et al. 1994; Herce and Garcia 2007b; Silhol et al. 2002; Torchilin et al. 2001; Vives et al. 2003). In the last two decades, numerous natural and synthetic peptides, such as Tat, transportan, and polyamino acids (e.g., polyarginines

**Electronic supplementary material** The online version of this article (doi:10.1007/s00249-011-0685-4) contains supplementary material, which is available to authorized users.

A. Gupta · G. Bothun (✉)
Department of Chemical Engineering, University of Rhode Island, Kingston, RI 02881, USA
e-mail: bothun@egr.uri.edu

D. Mandal · Y. Ahmadibeni · K. Parang
Department of Biomedical and Pharmaceutical Sciences, University of Rhode Island, Kingston, RI 02881, USA

Y. Ahmadibeni
Department of Chemistry, Columbus State University, Columbus, GA 31907, USA

or polylysines), have been discovered or designed for intracellular delivery of a variety of therapeutic agents of varying size, including nucleic acids, proteins, polymers, and nanoparticles (e.g., quantum dots) (Chan et al. 2006; Reuter et al. 2009; Tung and Weissleder 2003). Developing transporters is critical, as many new therapeutics molecules are hydrophobic or anionic, and thus difficult to disperse in aqueous phases or to achieve a high degree of membrane translocation, respectively (Lundberg et al. 2007).

The mechanisms by which CPPs interact with and traverse cell membranes are complex and depend on many factors, including peptide size (Henriques et al. 2006), charge, degree of hydrophobicity (Kiyota et al. 1996), and secondary structure (Olofsson et al. 2007), and membrane composition, heterogeneity (e.g., presence of lipid domains), and phase state (Andrushchenko et al. 2008; Ziegler 2008). Cellular uptake of CPPs is generally attributed to energy-dependent or endocytotic pathways. However, there have been a number of reports demonstrating CPP uptake by energy-independent pathways, including membrane poration and the formation of transient membrane defects (Lindsay 2002). These passive uptake mechanisms occur due to electrostatic attraction between cationic peptide residues [i.e., arginines (Futaki 2002, 2005) and lysines (Reuter et al. 2009)] and negative charges within the lipid headgroups (Joliot and Prochiantz 2004). This occurs initially at the outer lipid leaflet of the bilayer, but extends to the inner lipid leaflet once the peptide is membrane bound (Tung and Weissleder 2003; Herce and Garcia 2007a; Chan et al. 2006). Hydrophobic interactions aid passive uptake by associating the peptide with the membrane lipid tail region. Hence, an understanding of how the balance of electrostatic and hydrophobic interactions control CPP–membrane interactions and membrane translocation can be used to create designer CPPs with specific membrane activity (Futaki 2005).

In addition to a facile route to modify electrostatic/hydrophobic balance, the ideal CPP ligand or transporter would be small, stable, water soluble, easy to produce, and inexpensive (Hale and Hancock 2007). To this end, Ye et al. introduced a new class of low-molecular-weight (<1,000 MW) water-soluble cationic tripodal linear peptide analogs (LPA) that demonstrated cellular uptake via an energy-independent mechanism (Ye et al. 2007). These LPAs were engineered based on the positively charged phosphotyrosine binding pocket of the Src SH2 domain. LPAs constitute three positively charged L-amino acids linked through two alkyl chains (Arg-$C_n$-Arg-$C_n$-Lys, where $n = 4$–11). LPA-$C_{11}$ was able to deliver the negatively charged fluorescent phosphopeptide F-GpYEEI into human breast cancer BT-20 cells by possessing enough hydrophobicity for membrane translocation. However, comparative assessment of cell uptake by a F-LPA series has not been conducted, and cell uptake specificity has not been examined.

Previous studies on membrane activity of LPA-$C_4$, LPA-$C_7$, and LPA-$C_{11}$ were conducted with dipalmitoyl phosphatidylcholine/dipalmitoylphosphatidylglycerol (DPPC/DPPG, 70/30 and 85/15) liposomes as a bacterial cell membrane model system (Ye et al. 2010). These results suggested that the LPAs were adsorbed on the membrane by electrostatic forces followed by permeation into the bilayer dictated by the length of the hydrophobic linkage. We concluded that the hydrophobicity of the peptides induces increased permeabilzation into the bilayers, causing a degree of peptide-induced loss in cell membrane integrity. This study demonstrated that the LPA were able to bind to and disrupt anionic membranes, but no insight was gained into their ability to translocate across cell membranes.

This work combines cellular uptake results with model membrane studies to understand the mechanism of LPA uptake. Uptake of fluorescein–LPA conjugates (F-LPAs) was examined in BT-20 and CCRF-CEM (leukemia cancer cells). Based on the observed nonendocytic and nonspecific uptake behavior, DPPC/dipalmitoylphosphatidylserine (DPPC/DPPS, 85/15) liposomes were used as a model to study LPA–membrane interactions (Fig. 1). Calorimetry, electron microscopy, and spectroscopy studies are combined to describe the effects of LPA electrostatic/hydrophobic balance on membrane phase behavior, structure, and permeability. Anionic PS lipids are present in mammalian cell membranes, primarily in the inner lipid leaflet (Lohner and Prenner 1999). Phosphatidylserine (PS) carries one negative charge at neutral pH and has both donor and acceptor groups that participate in intermolecular

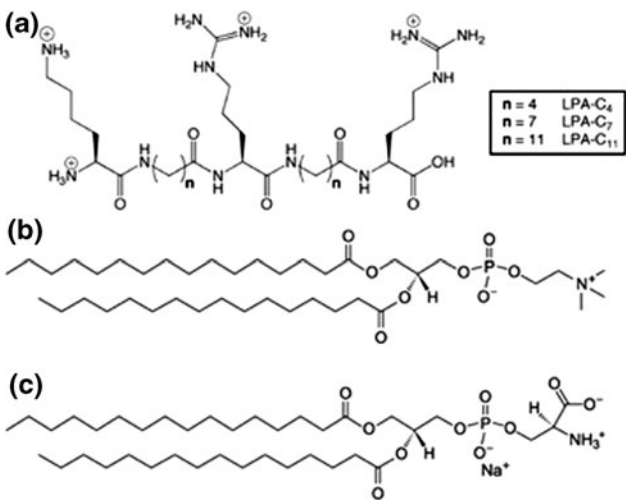


**Fig. 1** Chemical structures of **a** LPA-$C_n$, **b** DPPC, and **c** DPPS

headgroup hydrogen bonding. Phosphatidylcholine (PC)/PS membranes present a complex, biologically relevant system with strong cation dependence (De Pinto et al. 2007; Pandit et al. 2003).

## Experimental

### Materials

1,2-Dipalmitoyl-*sn*-glycero-3-phosphocholine (DPPC) dissolved in chloroform and 1,2-dipalmitoyl-*sn*-glycero-3-phosphoserine (DPPS) in chloroform/methanol (1:1 v/v) were purchased from Avanti Polar Lipids (Alabaster, AL). Carboxyfluorescein (FAM) was purchased from Sigma–Aldrich (St. Louis, MO). For peptide synthesis, Fmoc-L-amino acids and Fmoc-Arg(pbf)-Wang resin were purchased from Novabiochem (San Diego, CA). 2-(1*H*-Benzotriazole-1-yl)-1,1,3,3-tetramethyluronium hexafluorophosphate (HBTU), *N*-methylmorpholine (NMM), and piperidine were purchased from Sigma–Aldrich. All solvents were of high-performance liquid chromatography (HPLC) grade or higher. Sterile deionized ultrafiltered water was obtained from a Millipore Direct-3Q purification system.

### Peptide synthesis

LPAs were synthesized as previously described using a solid-phase synthesis strategy employing Fmoc-based chemistry and Fmoc-L-amino acid building blocks (Ye et al. 2007, 2010). Briefly, Fmoc-Arg(pbf)-Wang resin was used as the starting amino acid; Fmoc-Arg(pbf)-OH, Fmoc-Lys(Boc)-OH, and FmocNH$(CH_2)_n$COOH ($n = 4$, 7 or 11) were used as building blocks, and HBTU and NMM in dimethylformamide (DMF) were used as coupling and activating agents. Fmoc deprotection at each step was carried out in the presence of piperidine in DMF (20% v/v). A mixture of trifluoroacetic acid/ansiole/water (90:5:5 v/v/v) was used for side-chain deprotection and the final cleavage of the synthesized peptide from the solid support. Crude peptides were precipitated by adding cold ethyl ether and were purified by preparative reversed-phase high-performance liquid chromatography (HPLC) (Shimadzu LC-8A) on a Phenomenex-Gemini C18 column (10 μm, 250 × 21.2 mm). The purity of the final products (>95%) was confirmed by HPLC. The chemical structures of compounds were determined by a surface-enhanced laser desorption/ionization time-of-flight (SELDI-TOF) mass spectrometer on a Ciphergen protein chip instrument using α-cyano-4-hydroxycinnamic as a matrix.

The fluorescent probes were synthesized by coupling 5(6)-carboxyfluorescein diisobutyrate (CFDI, US Biological) with a Wang resin-bound LPA. This was achieved by adding resin-bound LPA (0.1 mmol) to a solution of CFDI (258 mg, 0.5 mmol), benzotriazol-1-yl-oxytripyrrolidinophosphonium hexafluorophosphate (PyBOP, 260.1 mg, 0.5 mmol), 1-hydroxy-7-azabenzotriazole (HOAt, 68.0 mg, 0.5 mmol), and *N*,*N*-diisopropylethylamine (DIPEA, 75 μl, 1.0 mmol) in dry DMF (10.0 ml). The mixture was shaken for 3 h at room temperature and then filtered and washed with DMF. The ester group of carboxyfluorescein was deprotected with 20% piperidine for 1 h. F-LPA was cleaved from the resin using trifluoroacetic acid (TFA)/thioanisole/dithiothreitol (DTT)/anisole (90:5:3: 2 v/v/v/v) over 2 h. The filtrate was collected, concentrated, and precipitated from cold ether, and the crude product was purified by preparative reversed-phase HPLC. The chemical structures of the F-LPAs were determined by surface-enhanced laser desorption/ionization time-of-flight mass spectrometry (SELDI-TOF–MS, Ciphergen ProteinChip®) (*m*/*z*): F-LPA-$C_{11}$: $C_{65}H_{97}N_{13}O_{13}$ calculated (calc) = 1,267.7; found = 1,267.2 $[M]^+$, 1,289.2 $[M + Na]^+$, 1,305.4 $[M + K]^+$; F-LPA-$C_7$: $C_{53}H_{74}N_{12}O_{12}$ calc = 1,070.5; found = 1,070.1 $[M]^+$, 1,091.7 $[M + Na]^+$, 1,108.1 $[M + K]^+$; F-LPA-$C_4$: $C_{49}H_{66}N_{12}O_{12}$ calc = 1,014.5; found, 1,014.9 $[M]^+$, 1,036.4 $[M + Na]^+$, 1,052.8 $[M + K]^+$. A schematic of F-LPA synthesis is shown in the Supplementary Material (Fig. S1).

### Cellular uptake assay

Human breast carcinoma cells BT-20 [American Type Culture Collection (ATCC) no. HTB-19] and leukemia cells CCRF-CEM (ATCC no. CCL-119) were grown in a 75-$cm^2$ cell culture flask with Eagle's minimal essential medium (EMEM) and Roswell Park Memorial Institute (RPMI) medium, respectively, in the presence of 10% fetal bovine serum (FBS). BT-20 cells were seeded in a six-well plate at density of $10^5$ cells per well with EMEM and allowed to grow for 24 h. After 24 h the medium was removed, the cells were washed with serum-free medium (SFM), and F-LPAs in SFM containing 0.5% dimethyl sulfoxide (DMSO) (v/v) were added at 50 μM to the cells for 1 h. In the case of leukemia cells, they were harvested and seeded in a six-well plate at a density of $10^7$ cells. DMSO (0.5% in SFM) and FAM (50 μM) were used as negative controls. The cells were incubated for 1 h at 37°C or 4°C. After 1 h incubation the medium was removed and cells were collected by centrifugation at 2,500 rpm for 5 min. They were then treated with 0.25% trypsin/0.53 mM ethylenediamine tetraacetic acid (EDTA) for 5 min followed by washing twice with phosphate-buffered saline (PBS). Finally, the cells were resuspended in flow cytometry buffer and analyzed by flow cytometry (FACSCalibur™, Becton–Dickinson) using fluorescein isothiocyanate (FITC) channel and CellQuest software. The data presented are based on the mean fluorescence signal for

5,000 cells collected. All assays were performed in triplicate.

### Liposome preparation

DPPC/DPPS (10 mM, 85/15) liposomes were prepared by mixing pertinent aliquots of DPPC and DPPS stock solutions in round-bottomed glass tubes and evaporating the solvents under a continuous stream of nitrogen. The tubes with dry lipid films were placed under vacuum for 1 h to remove residual solvent. The films were hydrated with deionized (DI) water at 55°C, vortexed, and extruded 15 times through 100-nm polycarbonate membranes at 55°C to yield unilamellar liposomes.

Carboxyfluorescein (FAM)-loaded encapsulated DPPC/DPPS liposomes were prepared by hydrating with 50 mM CF in pH 7.4 phosphate-buffered saline (PBS). The sample was subjected to five heat/cool thawing cycles at 55°C and 0°C, respectively. CF encapsulated liposomes were extruded as previously described. Unencapsulated CF was removed by gel filtration over a Sephadex G-25 coarse column (Sigma–Aldrich).

### Differential scanning calorimetry

DSC studies were carried out on a low-noise (±15 nW) TA Instruments Nano DSC with a 0.33 ml cell volume. The effects of the LPAs on the thermotropic phase behavior of DPPC/DPPS was examined by adding LPA to preformed liposomes at 3 and 30 mol% relative to total lipid (10 mM), which was equivalent to 0.3 and 4.3 mM LPA, respectively. The sample was immediately placed in the DSC and subjected to five heat/cool cycles in the range of 15–60°C at a rate of 1°C/min. This was done to observe the effects of lipid melting cycle on LPA interactions. During the initial heating steps, LPAs were only present outside of the liposomes and bound to the outer membrane leaflet.

### Cryogenic transmission electron microscopy

Cryo-TEM analysis was conducted on a JEOL JEM 2100 (Tokyo, Japan) operating at 80 kV. A thin film of the mixtures of the vesicles and the LPA samples at 10 mM was prepared on a copper grid coated with perforated carbon by blotting technique achieved in a chamber kept at 55°C and relative humidity of 100%. Excess sample was removed from the grid by absorbing with filter paper, and vitrification was effected by immersing the grid into a liquid ethane enclosure retained at a temperature just below its freezing point. The vitrified samples were maintained below −190°C during both transfer of the sample to the TEM and imaging to prevent sample deterioration. LPAs (30 mol% or 4.3 mM) were added to DPPC/DPPS liposomes at room temperature (gel phase, 10 mM). The samples were prepared in a cryopreparation chamber at 100% relative humidity and incubated at 55°C. Samples were transferred to, stored, and analyzed under liquid nitrogen. Compared with DSC studies, these samples represent fluid-phase liposomes after the first heating scan.

### Carboxyfluorescein leakage studies

FAM leakage experiments were conducted at 25°C and 55°C on a Perkin-Elmer LS 55 fluorescence spectrometer (Waltham, MA). CF encapsulated liposomes (2 μl) were added to a cell containing 3 ml PBS to yield 6.7 μM lipid. After 1,200 s, an aliquot of LPA in water was added to the cell to yield 30 mol% LPA relative to lipid (2.9 μM LPA). Triton X-100 (1.4 μl; Eastman Kodak Company, Rochester, NY, USA) was added after 3,600 s to solubilize the liposomes and release the FAM. Fluorescence intensities were measured at 0.01-min intervals with excitation and emission wavelengths set at 490 and 520 nm, respectively, and excitation and emission slit widths of 5 nm (Rex 1996).

## Results

### Cellular uptake

F-LPA uptake was examined in two different cell lines: BT-20 and CCRF-CEM. For BT-20 cells at 37°C, significant uptake of F-LPA-$C_{11}$ was observed relative to the DMSO (26.6-fold) and FAM (5.3-fold) controls (Fig. 2a). In contrast, there was no significant difference between the uptake of FAM compared with F-LPA-$C_7$ and F-LPA-$C_4$. At 4°C, a temperature that abolishes active transport mechanisms involved in endocytosis, F-LPA-$C_{11}$ uptake was still observed, though reduced threefold relative to 37°C. Uptake of F-LPA-$C_7$ and F-LPA-$C_4$ was negligible at 4°C.

F-LPA uptake by CCRF-CEM cells was conducted at 37°C. As with BT-20 cells, F-LPA-$C_7$ and F-LPA-$C_4$ uptake was the same as FAM (Fig. 2b). Only F-LPA-$C_{11}$ exhibited significant uptake relative to DMSO (60.5-fold) and FAM (16.8-fold). Uptake results for BT-20 and CCRF-CEM were similar for both cell lines, which suggests that the LPA hydrophobic/hydrophilic balance or degree of hydrophobicity is the primary factor governing membrane translocation.

### Characterization for membrane studies

Dynamic light scattering (DLS) results at 1 mM LPA in DI water showed that the LPAs did not self-associate. The

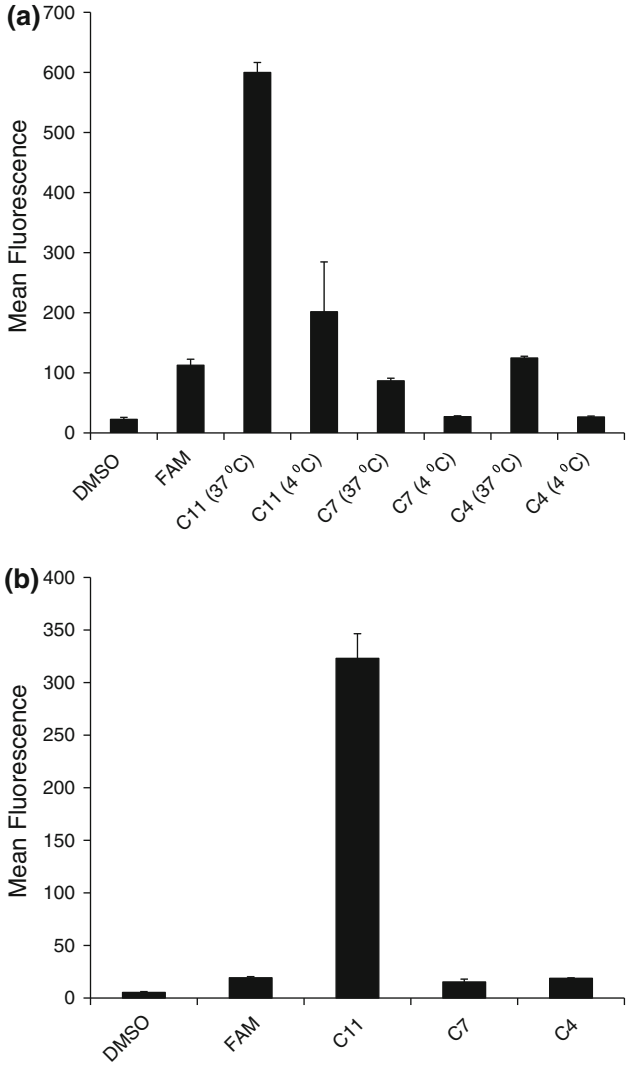


**Fig. 2** Cellular uptake of F-LPA-$C_4$, F-LPA-$C_7$, and F-LPA-$C_{11}$ (50 μM) relative to the unligated FAM fluorophore by **a** BT-20 at 4°C and 37°C and **b** CCRF-CEM cells at 37°C. Fluorescence-activated cell sorting (FACS) analysis was performed after incubating the cells with F-LPAs for 1 h

average hydrodynamic diameters were $0.7 \pm 0.1$, $0.8 \pm 0.1$, and $1.3 \pm 0.2$ nm for LPA-$C_4$, LPA-$C_7$, and LPA-$C_{11}$, respectively. These diameters are consistent with the lengths of $C_4$, $C_7$, and $C_{11}$ chains in all-*trans* configuration (0.5, 0.9, and 1.4 nm based on $0.127n$). Circular dichroism showed that only LPA-$C_{11}$ exhibited secondary structure (partial $\beta$-sheet conformation), consistent with previous results (Ye et al. 2007). The zeta potential of all LPAs was $12.4 \pm 2.3$ mV, confirming their cationic nature. Comparatively, the *z*-averaged hydrodynamic diameter and zeta potential for the DPPC/DPPS liposomes were $135.4 \pm 13.1$ nm and $-58.3 \pm 4.1$ mV, respectively. DLS and circular dichroism (CD) (Fig. S2) are described in the Supplementary Material.

## Differential scanning calorimetry: membrane phase behavior

DSC was first used to determine the effect of LPA binding on DPPC/DPPS membranes. Pure DPPC/DPPS (85/15) exhibited a gel to rippled gel pretransition at 38°C and a main gel to fluid phase transition or melting temperature at 42.5°C. No significant changes were observed over seven consecutive heat/cool cycles. Based on the melting temperatures of DPPC (41°C) and DPPS (53°C), the melting temperature for DPPC/DPPS liposomes represented the weighted average of the constituent lipids. This suggests that the lipids were well mixed with no apparent phase separation (Baciu and May 2004). Furthermore, pure LPAs did not show any phase transition within the temperature range examined (15–55°C).

Figure 3 shows the thermographs of 3 and 30 mol% LPAs added to preformed DPPC/DPPS liposomes at heating scans 1 through 5. Heating scans 4 (shown in blue) and 5 (shown in black) yielded similar thermograms, indicating that the systems were approaching a pseudo-equilibrium state. At 3 mol% LPA-$C_4$ and LPA-$C_7$ the first heating scan showed a slight increase in pretransition to 38.6°C, and a broad main transition composed of three convoluted peaks at 42.5°C, 43.5°C, and 46.5°C. With advancing heating scans, the pretransition disappeared and lipid melting resolved into broad peaks near 41°C and 48°C. These broad peaks denote melting with low cooperativity in DPPC- and DPPS-rich regions, respectively. The addition of 3 mol% LPA-$C_{11}$ yielded a pretransition at 38°C that was diminished with subsequent heating cycles. The main transition peak exhibited a shoulder near 46°C that became more pronounced with each heating scan. At 3 mol%, LPA-$C_{11}$ did not lead to higher temperature peak shifts as observed for LPA-$C_4$ and LPA-$C_7$.

Increasing LPA concentration from 3 to 30 mol% produced discernible changes in the phase behavior. Pretransitions were not observed even during the initial heating scans. LPA-$C_4$ and LPA-$C_7$ at 30 mol% caused lipid ordering as evident by the high-temperature convoluted melting peaks with low melting cooperativity. At 30 mol% LPA-$C_{11}$, the first heating scan was identical to that at 3 mol%. With progressing heating scans, LPA-$C_{11}$ caused phase separation similar to that of LPA-$C_4$ and LPA-$C_7$.

## Cryo-TEM: liposome structure

Cryo-TEM studies were carried out to determine the effects of LPA binding on liposome morphology. Compared with the DSC studies, these samples represent fluid-phase liposomes after the first temperature scan. The images presented are representative of structures consistent throughout the grid (Fig. 4).

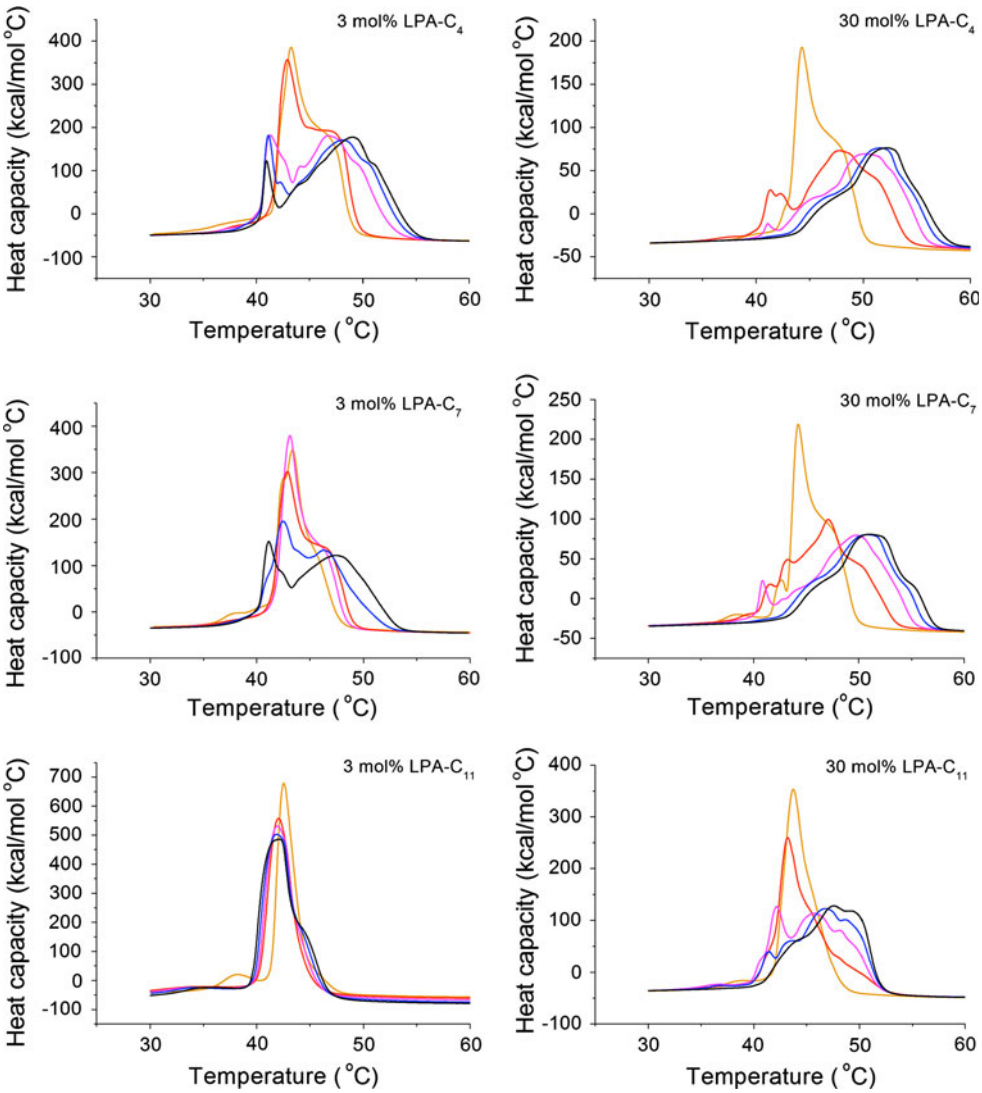


**Fig. 3** DSC thermographs of 10 mM DPPC/DPPS (85/15) with 3 and 30 mol% LPA-$C_4$ (*top two*), LPA-$C_7$ (*middle two*), and LPA-$C_{11}$ (*lower two*). Heating scans 1 (*orange*), 2 (*red*), 3 (*pink*), 4 (*blue*), and 5 (*black*) are shown

DPPC/DPPS liposomes were largely unilamellar with an average diameter consistent with DLS (134.5 nm). Addition of 30 mol% LPA-$C_4$ and LPA-$C_7$ caused an increase in liposome diameter ($C_7 > C_4$), which suggests that LPA binding led to bilayer expansion and liposome swelling. In turn, holes within the bilayer were observed after addition of 30 mol% LPA-$C_{11}$ (Fig. 4, open arrow) as well as notable membrane thinning and liposome disintegration (Fig. 4, black arrow). This was confirmed by the presence of unenclosed liposomes and bilayer fragments (Fig. 4, white arrows).

Fluorescence leakage: bilayer permeabilization

Bilayer permeabilization by LPAs was assessed by FAM leakage. Figure 5 shows plots of the percentage of FAM leakage as a function of time, expressed as $(I_0 - I_t)/(I_0 - I_{max})$, where $I_0$ is the initial fluorescence intensity and $I_{max}$ is the maximum fluorescence intensity when the liposomes were solubilized. Results from 0 to 1,200 s and 1,200 to 3,600 s denote spontaneous liposome leakage and LPA-induced leakage, respectively.

At 25°C, addition of LPA-$C_4$ and $C_7$ had no discernible effect on FAM leakage, while LPA-$C_{11}$ led to significant leakage (100% near 3,000 s). Similar results were observed for LPA-$C_4$ and LPA-$C_7$ at 55°C. However, the effect of LPA-$C_{11}$ on leakage at 55°C was even more pronounced than at 25°C, and is consistent with cryo-TEM results depicting liposome disintegration. These results demonstrate that LPA-$C_{11}$ causes bilayer permeabilization in both gel and fluid phases, while the effects of LPA-$C_4$ and LPA-$C_7$ are negligible.

## Discussion

Ye et al. (2007) demonstrated that F-LPA-$C_{11}$ efficiently entered BT-20 cells. However, the ability of LPAs with

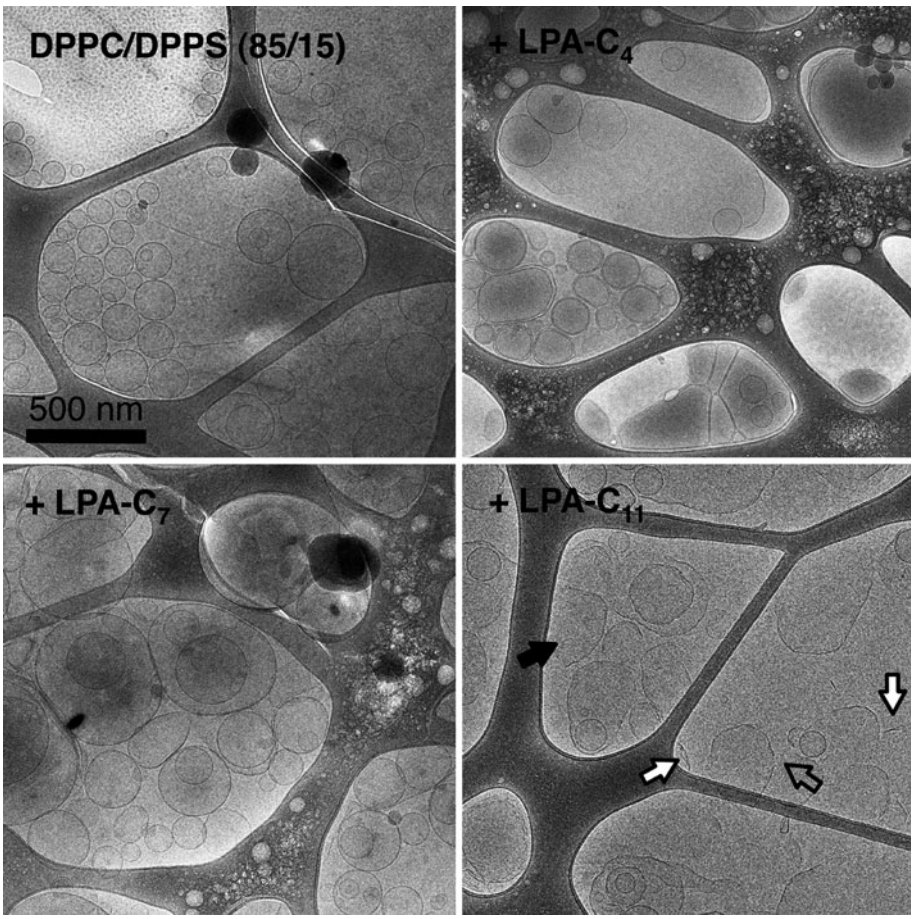


**Fig. 4** Cryo-TEM micrographs of DPPC/DPPS (85/15) liposomes exposed to 30 mol% LPA-$C_4$, LPA-$C_7$, and LPA-$C_{11}$ at 55°C (i.e., fluid-phase membranes). The *black arrow* denotes liposome disintegration, the *open arrow* denotes pore formation, and the *white arrows* denote bilayer fragmentation

shorter hydrophobic spacers (F-LPA-$C_4$ and F-LPA-$C_7$) for cell internalization was not investigated. Furthermore, no insight has been gained regarding cell specificity for any LPA species. In this work, fluorescein conjugates of LPA-$C_4$ (F-LPA-$C_4$) and LPA-$C_7$ (F-LPA-$C_7$) were synthesized, and their cellular uptake was compared with that of F-LPA-$C_{11}$ using BT-20 and CCRF-CEM cells. Inhibited uptake at 4°C coupled with previous studies showing that the presence of sodium azide [adenosine triphosphate (ATP) depletion] did not inhibit internalization of F-LPA-$C_{11}$ suggests that its uptake is nonspecific and nonendocytic (Ye et al. 2007; Fawell et al. 1994). The fact that only F-LPA-$C_{11}$ achieved appreciable uptake by BT-20 and CCRF-CEM cells relative to LPAs with shorter alkyl linkages, F-LPA-$C_4$ and F-LPA-$C_7$, shows that sufficient hydrophobicity is required. We have previously characterized the hydrophobic/hydrophilic balance of these based on the ratio of the van der Waals areas of the hydrophobic linkages to that of the polar regions (0.7, 1.1, and 1.8 for LPA-$C_4$, LPA-$C_7$, and LPA-$C_{11}$, respectively) (Ye et al. 2010). As discussed below, the cellular uptake results correlate with the disruptive behavior of LPAs on model DPPC/DPPS membranes.

The role of LPA hydrophobicity is depicted by changes in phase behavior caused by LPA-$C_{11}$. At 3 mol% LPA-$C_{11}$ relative to lipid, which corresponds to a DPPS-to-LPA ratio of 5:1 (excess DPPS relative to LPA), a main transition peak was observed at 42°C and a shoulder peak at ~45°C. The main peak is shifted by −0.5°C relative to pure DPPC/DPPS. These results suggest that LPA-$C_{11}$ led to partial phase separation relative to pure DPPC/DPPS, but mixed within the phases through hydrophobic LPA alkyl ($C_{11}$)–lipid acyl tail ($C_{16}$) interactions. In contrast, LPA-$C_4$ and LPA-$C_7$ at 3 mol% led to considerable phase separation that became more pronounced with progressive heating scans. Their binding resulted in transitions that are reminiscent of the pure lipids, which suggests that they are likely to be bound externally to DPPS-rich domains (Schwieger and Blume 2007). Hence, LPA-$C_4$ and LPA-$C_7$ anchored at the lipid–water interface, while LPA-$C_{11}$ penetrated into the membrane.

Increasing LPA concentration to 30 mol% corresponded to a DPPS-to-LPA ratio of 1:2 (excess LPA relative to DPPS). At this saturated condition, the broad main transition peaks were shifted to higher temperatures for all LPAs, with LPA-$C_4$ and LPA-$C_7$ causing a slightly greater shift

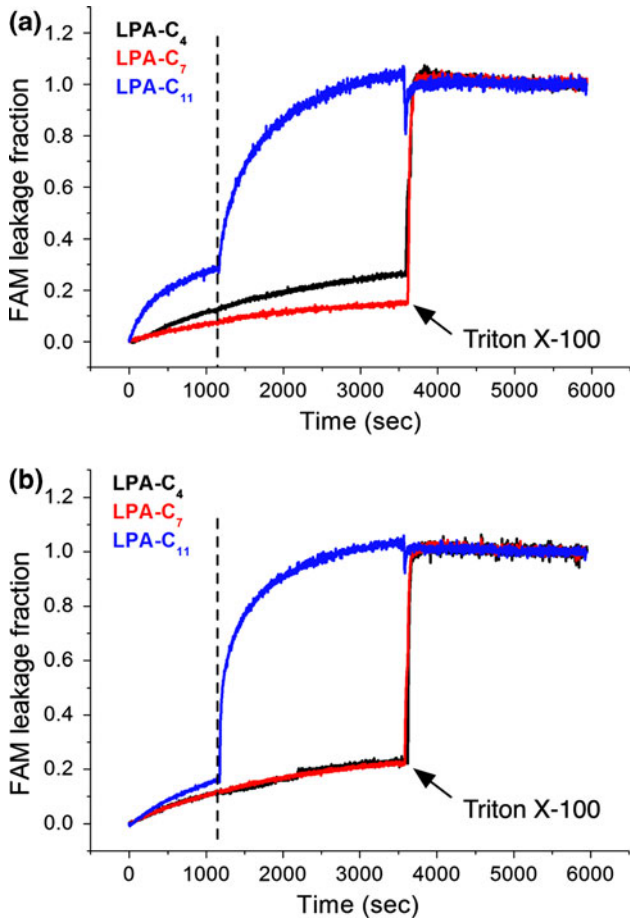


**Fig. 5** Carboxyfluorescein (FAM) leakage from DPPC/DPPS (85/15) liposomes at **a** 25°C (gel phase) and **b** 55°C (fluid phase) in the presence of LPA-$C_4$ (*black*), LPA-$C_7$ (*red*), and LPA-$C_{11}$ (*blue*). The *dashed vertical line* denotes addition of LPA and the *arrows* denote addition of Triton X-100

than LPA-$C_{11}$. Previous work on DPPC/DPPS phase behavior has shown that charge shielding of electrostatic repulsion between DPPS molecules due to peptide binding can reinforce hydrophobic interactions between acyl chains and that partial dehydration of the membrane can occur due to peptide binding (Sevcsik et al. 2008; Bouffioux et al. 2007). These interactions were enhanced when going from 3 to 30 mol% LPA. Both mechanisms can lead to an increase in lipid melting temperature and reflect the interfacial properties of LPAs on DPPC/DPPS membranes.

To provide further insight into binding affinity, isothermal titration calorimetry was conducted at 55°C (fluid liposomes). Preliminary results at low LPA-to-lipid molar ratios (up to 0.2 mol% LPA relative to lipid) provide evidence of the extent of LPA binding (see Supplementary Material, Fig. S3). LPA-$C_4$ and LPA-$C_7$ exhibited exothermic binding, consistent with electrostatic interactions, and the binding enthalpy decreased with increasing LPA concentration. In contrast, LPA-$C_{11}$ exhibited endothermic binding, consistent with hydrophobic interactions, and the binding enthalpy did not decrease with LPA concentration. These results confirm the role of LPA hydrophobicity in membrane binding, and further show that the effects of LPA-$C_{11}$ are likely due to greater binding affinity.

Despite the ability of LPAs to disrupt DPPC/DPPS membrane phase behavior, as inferred from DSC results, only LPA-$C_{11}$ led to significant morphological changes in DPPC/DPPS liposomes. Hydrophobicity, which drove LPA-$C_{11}$ insertion into the membranes, also led to membrane disintegration, as revealed by cryo-TEM. While this analysis was conducted at high LPA concentration (30 mol%), it demonstrates the ability for LPA-$C_{11}$ to create holes within and breach the membrane. In contrast, no holes, fragmentation or significant changes in DPPC/DPPS liposome structure were observed in the presence of LPA-$C_4$ or LPA-$C_7$. It is likely that LPA-$C_{11}$ surrounded the edges of these fragments, which is consistent with similar observations reported by Sevcsik et al. (2008) and Johnsson and Edwards (2003) for an equimolar mixture of DPPC/DPPS in the presence of 4 mol% LL-37, a human multifunctional peptide.

It is important to note that cryo-TEM analysis was performed on pseudoequilibrated samples (i.e., samples analyzed 10 min after LPA addition). Comparatively, fluorescence leakage results, which captured the effects of the initial binding event on membrane permeabilization, demonstrated that LPA-$C_{11}$ led to rapid permeabilization of DPPC/DPPS liposomes in both the gel and fluid phases. In contrast, LPA-$C_4$ and LPA-$C_7$ had a negligible effect on permeabilization in either phase due to their anchoring at the lipid–water interface. The permeabilizing effects of LPA-$C_{11}$ can be attributed to membrane pore formation followed by liposome disintegration.

A mechanism for nonendocytic uptake of F-LPA-$C_{11}$ (i.e., LPA-$C_{11}$ as a membrane translocating ligand) is proposed based on the model membrane studies. Electrostatic interactions facilitated LPA binding to the cell membranes; however, only LPA-$C_{11}$ with sufficient hydrophobicity penetrated into the membranes and remained with the cells after washing. At a critical F-LPA-$C_{11}$ concentration (currently under investigation), this led to the formation of transient holes or voids that aided translocation across the membranes. It is known that secondary solution structure and changes in peptide conformation upon membrane binding correlate to membrane activity (Magzoub et al. 2001; Deshayes et al. 2004). However, at this stage we cannot comment on the exact role that LPA-$C_{11}$ conformation plays in facilitating uptake.

## Conclusions

Differential nonendocytic cellular uptake has been demonstrated for LPA–fluorophore conjugates by varying the length of the hydrophobic LPA alkyl linkage. Uptake was consistent with DSC, cryo-TEM, and fluorescence leakage results obtained through LPA–model membrane studies. Our results indicate that electrostatic attraction facilitates LPA binding to anionic DPPC/DPPS membranes and that the degree of LPA hydrophobicity, based on alkyl linker length, determines the degree of membrane penetration and translocation. This is consistent with our previous work that indicated minimal binding to zwitterionic DPPC liposomes based on DSC and membrane permeabilization (Ye et al. 2010). Strong electrostatic interactions, coupled with LPA-$C_{11}$ hydrophobicity, led to membrane phase separation, permeabilization, and disintegration. While the model membrane studies were conducted at high concentrations relative to therapeutically relevant concentrations, they infer a transient hole or void formation mechanism that facilitated uptake of the LPA-$C_{11}$ conjugate. Our work shows that differential uptake of LPA conjugates can be achieved by manipulating the balance of electrostatic and hydrophobic contributions. While LPAs represent "simple" short peptides, they combine both water-solubility and tunable membrane activity, which are important for achieving high bioavailability and intracellular delivery.

**Acknowledgments** We acknowledge financial support from American Cancer Society grant RSG-07-290-01-CDD and National Science Foundation grant CHE 0748555.

## References

Andrushchenko VV, Aarabi MH, Nguyen LT, Prenner EJ, Vogel HJ (2008) Thermodynamics of the interactioc of tryptophan-rich cathelicidin antimicrobial peptides with model and natural membranes. Biochim Biophys Acta 1778:1004–1014

Baciu CL, May S (2004) Stability of charged, mixed lipid bilayers: effect of electrostatic coupling between the monolayers. J Phys Condens Matter 16:455–460

Bouffioux O, Berquand A, Eeman M, Paquot M, Fufrene YF, Brasseur R, Deleu M (2007) Molecular organization of surfactin-phospholipid monolayers: effect of phospholipid chain length and polar head. Biochim Biophys Acta 1768:758–768

Chan DI, Prenner EJ, Vogel HJ (2006) Tryptophan- and arginine-rich antimicrobial peptides: structures and mechanisms of action. Biochim Biophys Acta 1758(9):184–202

De Pinto V, Tomasello F, Messina A, Guarino F, Benz R, La Mendola D, Magri A, Milardi D, Pappalardo G (2007) Determination of the conformation of the human VDAC1 N-terminal peptide, a protein moiety essential for the functional properties of the pore. Chem Bio Chem 8(7):744–756

Deshayes S, Heitz A, Morris MC, Charnet P, Divita G, Heitz F (2004) Insight into the mechanism of internalization of the cell-penetrating carrier peptide Pep-1 through conformational analysis. Biochemistry 43:449–457

Deshayes S, Morris MC, Divita G, Heitz F (2005) Cell-penetrating peptides: tools for intracellular delivery of therapeutics. Cell Mol Life Sci 62(16):1839–1849

El-Andaloussi S, Holm T, Langel U (2005) Cell-penetrating peptides: mechanisms and applications. Curr Pharm Des 11(28):3597–3611

Fawell S, Seery J, Daikh Y, Moore C, Chen LL, Pepinsky B, Barsoum J (1994) Tat-mediated delivery of heterologous proteins into cells. Proc Natl Acad Sci USA 91(2):664–668

Futaki S (2002) Arginine-rich peptides:potential for intracellular delivery of macromolecules and the mystery of the translocation mechanisms. Int J Pharm 245:1–7

Futaki S (2005) Membrane permeable arginine rich peptides and the translocation mechanisms. Adv Drug Deliver Rev 57:547–558

Hale JD, Hancock RE (2007) Alternative mechanisms of action of cationic antimicrobial peptides on bacteria. Exp Rev Anti-Infect Ther 5(6):951–959

Henriques ST, Melo MN, Castanho MA (2006) Cell penetrating peptides and antimicrobial peptides: how different are they? Biochem J 399:1–7

Herce HD, Garcia AE (2007a) Cell penetrating peptides: how do they do it? J Biol Phys 33(5–6):345–356

Herce HD, Garcia AE (2007b) Molecular dynamics simulations suggest a mechanism for translocation of the HIV-1 TAT peptide across lipid membranes. Proc Natl Acad Sci USA 104(52):20805–20810

Johnsson M, Edwards K (2003) Liposomes, disks, and spherical micelles: aggregate structure in mixtures of gel phase phosphatidylcholines and poly (ethylene glycol)-phospholipids. Biophys J 85(6):839–847

Joliot A, Prochiantz A (2004) Transduction peptides: from technology to physiology. Nat Cell Biol 6(3):189–196

Kiyota T, Lee S, Sugihara G (1996) Design and synthesis of amphiphilic a-helical model peptides with systematically varied hydrophobic-hydrophilic balance and their interaction with lipid- and bio-membranes. Biochemistry 35:13196–13204

Lindsay MA (2002) Peptide-mediated cell delivery: application in protein target validation. Curr Opin Pharmacol 2:587–594

Lohner K, Prenner E (1999) Differential scanning calorimetry and X-ray diffraction studies of the specificity of the interaction of antimicrobial peptides with membrane-mimetic systems. Biochim Biophys Acta 1462:141–156

Lundberg P, El-Andaloussi S, Sutlu T, Johansson H, Langel U (2007) Delivery of short interfering RNA using endosomolytic cell-penetrating peptides. FASEB 21:664–671

Magzoub M, Kilk K, Eriksson LE, Langel U, Graslund A (2001) Interaction and structure of cell-penetrating peptides in the presence of phospholipid vesicles. Biochim Biophys Acta 1512:77–89

Olofsson A, Borowik T, Grobner G, Sauer-Eriksson AE (2007) Negatively charged phospholipid membranes induce amyloid formation of medin via an a-helical intermedicate. J Mol Biol 374:186–194

Pandit S, Bostick D, Berkowitz ML (2003) Mixed bilayer containing dipalmitoylphophatidylcholine and dipalmitolyphosphatidylserine: lipid complexation, ion binding and electrostatics. Biophys J 85:120–131

Patel LN, Zaro JL, Shen WC (2007) Cell penetrating peptides: intracellular pathways and pharmaceutical perspectives. Pharmaceut Res 24(11):1977–1992

Reuter M, Scwieger C, Meister A, Karlsson G, Blume A (2009) Poly-L-lysines and poly-L-arginines induce leakage of negatively charged phospholipid vesicles and translocate through the lipid bilayer upon electrostatic binding to the membrane. Biophys Chem 144:27–37

Rex S (1996) Pore formation induced by the peptide melittin in different lipid vesicle membranes. Biophys Chem 58(1–2):75–85

Schwieger C, Blume A (2007) Interaction of poly (L-lysines) with negatively charged membranes: an FT-IR and DSC study. Eur Biophys J 36(4–5):437–450

Sevcsik E, Pabst G, Richter W, Danner S, Amenitsch H, Lohner K (2008) Interaction of LL-37 with model membrane systems of different complexity influence of the lipid matrix. Biophys J 94:688–699

Silhol M, Tyagi M, Giacca M, Lebleu B, Vives E (2002) Different mechanisms for cellular internalization of the HIV-1 Tat-derived cell penetrating peptide and recombinant proteins fused to tat. Eur J Biochem 269(2):494–501

Stewart KM, Horton KL, Kelley SO (2008) Cell-penetrating peptides as delivery vehicles for biology and medicine. Org Biomol Chem 6(13):2242–2255

Torchilin VP, Rammohan R, Weissig V, Levchenko TS (2001) TAT peptide on the surface of liposomes affords their efficient intracellular delivery even at low temperature and in the presence of metabolic inhibitors. Proc Nat Acad Sci USA 98(15):8786–8791

Tung CH, Weissleder R (2003) Arginine containing peptides as delivery vectors. Adv Drug Deliv Rev 55(2):281–294

Vives E, Richard JP, Rispal C, Lebleu B (2003) TAT peptide internalization: seeking the mechanism of entry. Curr Protein Pept Sci 4(2):125–132

Vives E, Schmidt J, Pelegrin A (2008) Cell-penetrating and cell-targeting peptides in drug delivery. BBA-Rev Cancer 1786(2):126–138

Ye G, Nam NH, Kumar A, Saleh A, Shenoy DB, Amiji MM, Lin X, Sun G, Parang K (2007) Synthesis and evaluation of tripodal peptide analogues for cellular delivery of phosphopeptides. J Med Chem 50(15):604–617

Ye G, Gupta A, De Luca R, Parang K, Bothun GD (2010) Bilayer disruption and liposome restructuring by a homologous series of small arg-rich synthetic peptides. Colloid Surf B 76(1):76–81

Ziegler A (2008) Thermodynamic studies and binding mechanisms of cell-penetrating peptides with lipids and glycosaminoglycans. Adv Drug Del Rev 60(4–5):580–597